ENVIRONMENTAL IMPACT

Natural occurrences of asbestos (NOA) contain intermixed fiber morphologies and mineral polymorphs which may confound analytical results in investigations of NOA-impacted communities. In this study, electron microscopy techniques were employed to address potential analytical variability from intergrown serpentine mineral phases. Non-asbestos serpentine fibers were superficially similar to chrysotile but were differentiated quickly using modified transmission electron microscopy (TEM) methods. TEM subsamples contained smaller particles with potentially higher asbestos concentrations than polarized light microscopy (PLM) subsamples from the same rock. Scanning electron microscopy (SEM) of intermediate size ranges revealed complex NOA particles not resolved with PLM or TEM. These large particles are likely to exist in samples prepared by mechanical crushing or grinding, but are unlikely using "releasable asbestos" methods.

Analysis of Serpentine Polymorphs in Investigations of Natural Occurrences of Asbestos

Jeff Wagner

California Department of Public Health, Environmental Health Laboratory Branch, 850 Marina Bay Parkway, G365/EHLB, Richmond, CA 94804, USA. E-mail: jeff.wagner@cdph.ca.gov

ABSTRACT

This work investigates potential analytical variability in environmental investigations of natural occurrences of asbestos (NOA) due to intergrown serpentine minerals. Franciscan complex and serpentinite rock samples were obtained from likely NOA sites in coastal Northern California with geographic information system (GIS) maps, then analyzed using polarized light microscopy (PLM), transmission electron microscopy with energy-dispersive x-ray analysis and selected area electron diffraction (TEM /SAED/EDS), and environmental scanning electron microscopy with EDS (ESEM/EDS). Non- asbestos serpentine fibers were superficially similar to chrysotile but were differentiated quickly using TEM morphology criteria and reference SAED overlays. 94 NOA fibers were classified as asbestiform chrysotile (62%), polygonal serpentine (34%), lizardite scrolls (2%), and lizardite laths (2%). Chrysotile fibril widths (mean = 42 nm) were significantly different from those of polygonal serpentine and lizardite laths (167 and 505nm, respectively), but not lizardite scrolls (37nm). Due to differing preparations and microscope resolutions, TEM analyses investigated a distinct, smaller population of particles (0.01-10 um) than did PLM analyses (10-100 um). A higher proportion of asbestiform phases in the finer fraction could potentially bias TEM bulk percent asbestos determinations. ESEM/EDS of intermediate particle size ranges revealed 20-200 um, elongated particles with intermixed asbestiform and non-asbestiform structures on their surfaces. These particles were too thick and complex to be resolved by PLM, and too massive to be detected by TEM. These large particles are likely to exist in samples prepared by mechanical crushing or grinding, but are not likely to be generated by "releasable asbestos" methods.

Keywords: asbestos, NOA, naturally occurring asbestos, serpentine, chrysotile, Franciscan mélange, SEM, TEM, PLM, GIS.

INTRODUCTION

Concerns of potential health effects from disturbed, natural occurrences of asbestos (NOA, alternatively defined as "naturally occurring asbestos") have resulted in environmental investigations worldwide, including several Western US regions (Libby, Montana [1], El Dorado County, California [2], Swift Creek, Washington [3], and Boulder City, Nevada [4]). NOA refers here to asbestos that has not been extracted and refined for commercial purposes, but rather has been exposed unintentionally by excavation, road grading, or mining for other minerals (e.g., Libby vermiculite). NOA deposits are associated most frequently with ultramafic or serpentinite rock [5], and to a lesser extent, Franciscan assemblage and talc deposits [6] [7] [8] [9]. Disturbed NOA fibers are at risk to be dispersed into the air and off-site, especially if they are contained in soils of easily aerosolizable particle sizes, tracked out on construction vehicles, or located in dry, windy areas [4] [10].

NOA samples contain intermixed phases of different mineral polymorphs, chemical compositions, and fiber morphologies, which may lead to variable analytical results [11]. Compared to commercial asbestos products with more uniform fiber properties (e.g., [12]), NOA fibers are not as easily reconciled with conventional legal, health-based, or geological definitions of asbestos [13] [14] [15] [16]. The presence of asbestiform fibril morphology, typically defined as splayed ends, average aspect >20:1, and width < 500 nm, is a key determination for many NOA investigations [17] [18] [19].

Analyses of NOA aggregates typically are conducted with standard methods utilizing polarized light microscopy (PLM) or transmission electron microscopy with energy-dispersive x-ray analysis and selected-area electron diffraction (TEM/EDS/SAED) [8] [20] [18] [21]. PLM analyses (often supplemented with low-power stereozoom microscopy) are quick and inexpensive relative to TEM, but lack the spatial resolution to identify finely divided phases or fibril end morphology. More sensitive TEM/EDS/SAED identification methods [18] [21] [22] [23] have been recommended when PLM analyses of suspected NOA samples show zero to trace levels of asbestos [24]. However, TEM analyses typically involve very small subsample volumes, so sample homogenization is crucial if findings are applied to the sample as a whole [8] [25]. Both PLM and TEM are transmission techniques, and thus have potential difficulty with thick particles.

Scanning electron microscopy with EDS (SEM/EDS) is less frequently utilized in standard NOA quantitations [26] [27] [28] due to its inability to identify asbestos definitively. However, the reflective nature of SEM/EDS makes it is an excellent candidate for qualitative surface characterizations of thick particles with minimal sample preparation. SEM/EDS has been used to provide insights into geologic studies of amphiboles [4] [29] [30] [31] and serpentine minerals [32] [9] [33].

The various serpentine mineral structures have been refined in the mineralogy literature over the past 60 years (e.g., [34] [35]). These studies, often utilizing milled, thin sections to obtain optimal diffraction and imaging of serpentine fibers down their axes, have differentiated the layered structures of lizardite (flat sheets with in-plane rotations [8]), chrysotile (concentric, cylindrical or spiral sheets around an amorphous central core [36]), polygonal serpentine (flat

sheets arranged in ordered sectors around a hollow or chrysotile core [37]), and antigorite (corrugated sheets [38]).

In contrast, NOA preparations specified by environmental methods typically yield fibers which lie in their preferred orientations (viewed perpendicular to their fiber axes), and may be relatively thick. Further, environmental methods often use qualitative, visual SAED confirmations rather than more costly, multiple-zone-axis measurements for each fiber [22]. Qualitative similarities between different serpentine mineral SAEDs is a potential source of error, though superimposed film negatives of standard SAEDs on a light box have been used to help discriminate between them [39].

In this work, non-standard modifications of NOA analysis methods are used to investigate analytical challenges for environmental investigations of intergrown serpentine minerals. Franciscan Complex and Serpentinite rock samples were obtained from likely NOA sites in coastal Northern California with the aid of geographic information system (GIS) mapping. NOA samples were analyzed using PLM, TEM/ EDS with digital SAED overlays, and SEM/EDS.

METHODS

GIS-Assisted Environmental Sampling

Selection of NOA sampling locations was accomplished by first creating a map of likely NOA locations. Ultramafic and serpentinite are the most common NOA-containing rock types in California, primarily located within the Sierra and Cascade mountain ranges [8] [5]. Franciscan Complex rocks of the coastal ranges have also been reported to contain NOA, not only in the serpentinite rocks with which they are commonly associated, but also within Franciscan metamorphic schist and mélange, both of which are highly-sheared, tectonic mixtures of multiple rock types [40] [41].

A GIS map of potential California NOA locations was created using ArcMap (Redlands, CA) and publicly available geologic databases. Ultramafic rock data from the Geologic Map of California [42] [43] were mapped, along with locations of asbestos mines and other reported occurrences [44]. The asbestos occurrence data was then re-mapped by reported asbestos type (instead of mine type as in [5]), and Franciscan schist and mélange rock locations from the Geologic Map of California data were added (Fig. 1).

Serpentine rock regions often exhibit characteristic, chaparral-type vegetation [45]. Comparison between publicly available GIS vegetation data and serpentinite regions of Fig.1 confirmed this correlation in several regions of Northern California [46].

These maps and vegetation types were used to help locate potential NOA-bearing samples. Small rocks (2-4 cm in diameter) were collected from two locations from the Northern California coastal range with predominant serpentinite and Franciscan complex (mélange) rocks. This paper focuses on analyses of two rocks from Location 1 (Rocks A and B) and one rock from Location 2 (Rock C). Rocks A and B were predominantly light green and blue with angular fractures and
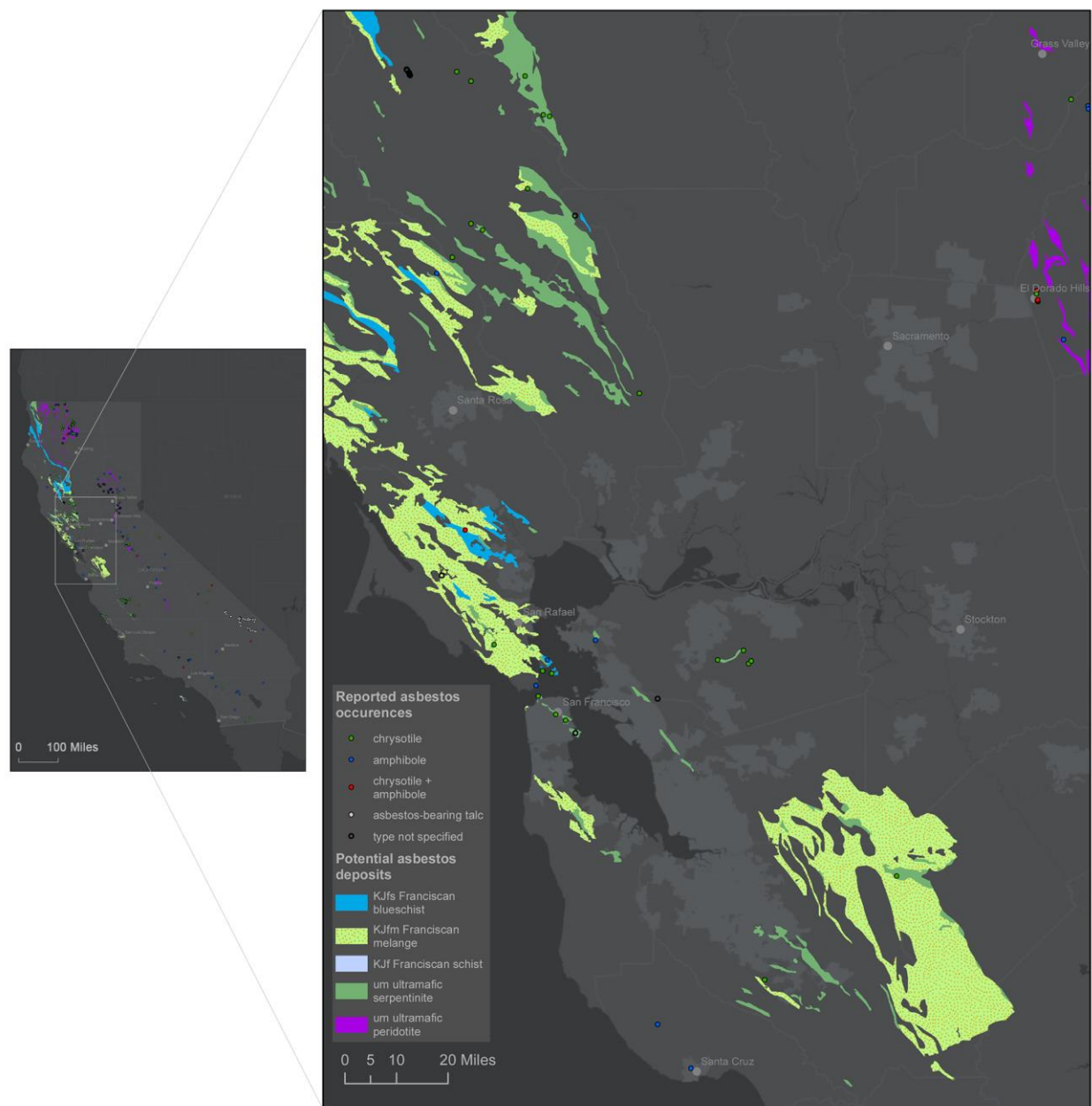
Figure 1. GIS map of potential NOA locations in California with enlarged view of San Francisco Bay Area and Sacramento. Light green and blue regions represent Franciscan Mélange and blueschist, respectively.

white veins (Figures 2a, 3a). Rock C was black and rounded, with dark green fracture lines (Figure 4a).

NOA subsamples were obtained from each rock by abrading the surfaces of cracks, veins, and other potentially fibrous regions with a clean stainless steel scalpel and forceps. These particles were then ground with a mortar and pestle in alcohol [18]. This approach differs from quantitative sampling methods in which representative rocks are obtained from a study area, and
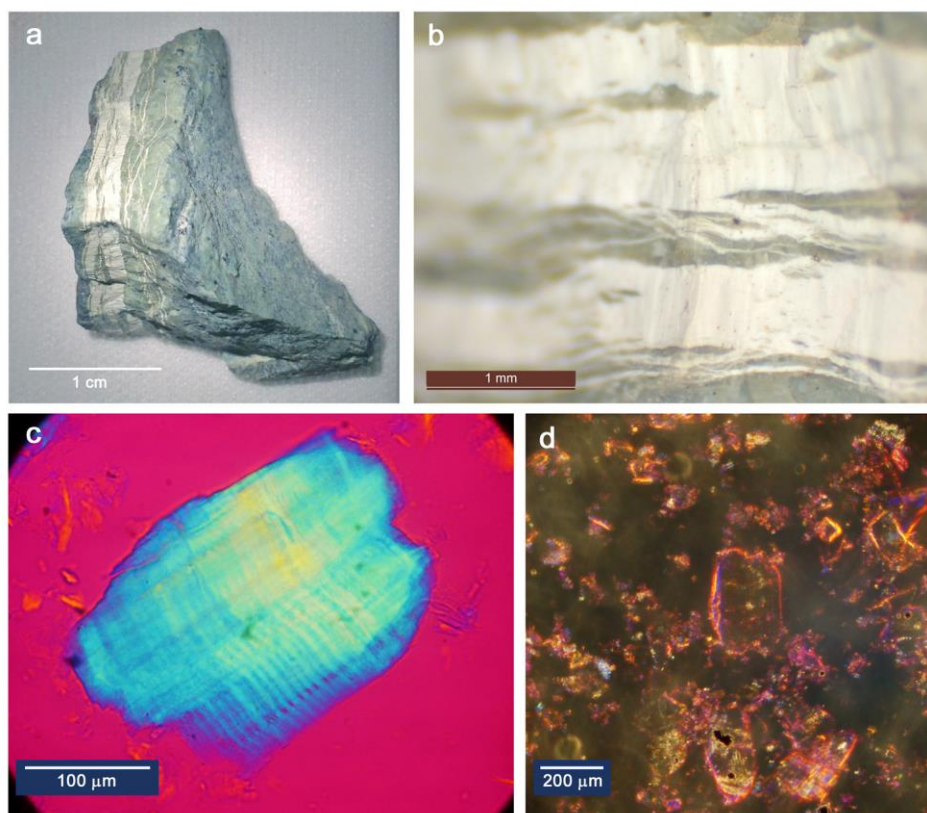
Figure 2. Rock A. a) Hand specimen. b) sub-sampled region yielding white flakes and powder when probed with tweezers (stereozoom microscope (SZM), 40x). c) plates with corrugated morphology (PLM with crossed polars and 1st-order red retardation plate (PLM/R1), 400x). d) thick plates with edge colors corresponding to $n_{d, \perp} = 1.56$, $n_{d, \parallel} = 1.57$ (PLM with dispersion staining objective (PLM/DS), 100x).

then pulverized and homogenized to obtain representative subsamples of those rocks. In contrast, the goal of this study was to purposely maximize the subsampling of fibrous NOA particles to evaluate NOA characterization methods.

Optical Microscopy

A stereozoom microscope (Leica S8APO) with digital camera (Leica DFC420) was used to record gross sample properties and prepare PLM subsamples.

NOA subsamples were placed in 1.550 refractive index oil (Cargille Laboratories, Cedar Grove, NJ) on slides with coverslips. PLM was conducted with a Nikon E600POL transmitted light microscope with digital camera (Nikon DS-Ri1 with DS-Ri1-U2 controller). Standard PLM methods were used to identify fibers by morphology, color under plane polarized light, extinction angle under crossed polarizers, sign of elongation using a full wave/1st-order retardation plate, and birefringence (= $n_{d, \parallel}$ - $n_{d, \perp}$, difference between indices of refraction in parallel and perpendicular orientations) as measured by dispersion staining [20] [18] [47].

Figure 3. Rock B. a) Hand specimen. b) Soft fibrous tufts (SZM, 80x). c) Splintery, brittle fibers (SZM, 80x). d) Asbestiform fiber bundles with positive sign of elongation from region (b) (PLM/R1, 400x). e) Birefringent bundles from region (b) with $n_{d, \perp}$ = 1.54, $n_{d, \parallel}$ = 1.55 (PLM/DS, 100x). f) Laths and ambiguous fiber bundles with positive sign of elongation from region (c) (PLM/R1, 100x). g) Birefringent pseudo-bundles from region (c) with $n_{d, \perp}$ = 1.56, $n_{d, \parallel}$ = 1.57 (PLM/DS, 100x).

TEM/SAED and STEM/EDS

TEM grids were prepared using one of two methods: 1) water filtration: 1.5 mg NOA subsample/water suspension transferred to 0.1 um polycarbonate filter, carbon coated, then cleared in a chloroform Jaffe washer [23], or 2) microdrop technique: one drop of NOA/alcohol suspension transferred directly to a formvar-supported grid (Carbon Type-B, Ted Pella) via pipet, then coated with evaporated carbon (Bal-Tec MED-020, Liechtenstein) [8]. TEM/SAED was conducted with an FEI Tecnai 12 with scanning TEM (STEM) unit, connected to a side-mounted CCD camera (Orius 830, Gatan, Pleasanton, CA) and EDS system with 80 mm^2 silicon drift X-ray detector (Aztec / 80T X-MAX, Oxford Instruments, Abingdon, UK). TEM imaging was conducted with a tungsten source at an accelerating voltage of 100kV. SAED patterns were obtained at a camera length of 660 mm. Gatan Digital Micrograph was used to
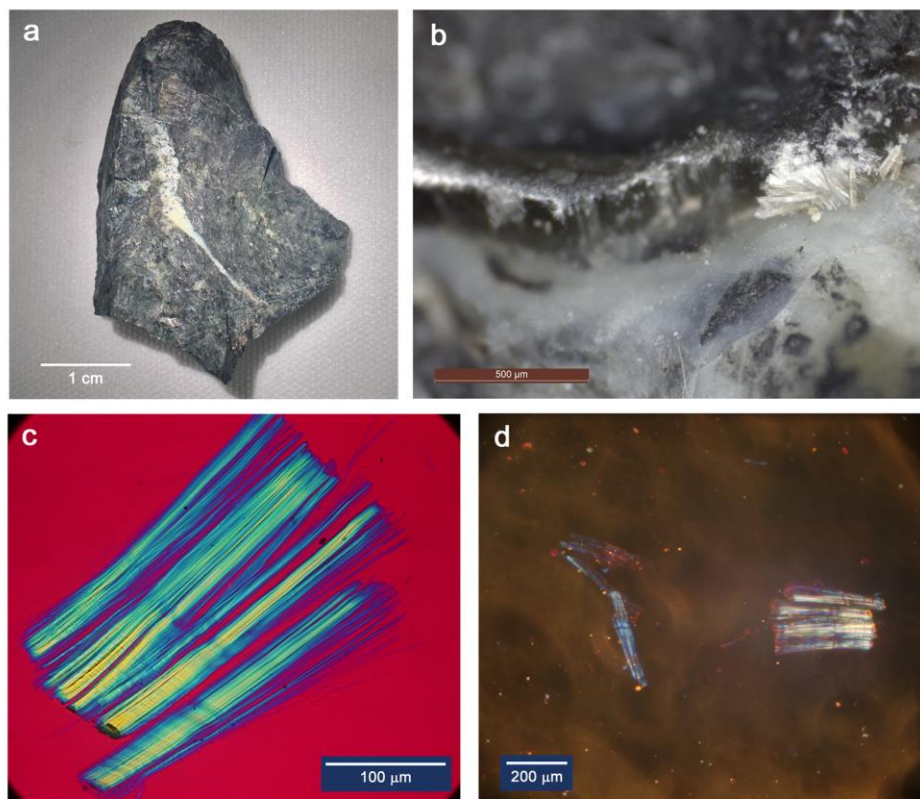
Figure 4. Rock C. a) Hand specimen. b) sub-sampled region within ridge exhibiting stiff, white fibers (SZM, 80x). c) Rigid bundles (PLM/R1, 400x). d) Some fibers showing $n_{d,\perp} = 1.55$, $n_{d,\parallel} = 1.56$; others too thick to exhibit DS colors (PLM/DS, 100x).

measure fiber widths and SAED patterns. EDS data were acquired from select regions of NOA particles in STEM mode.

A waffle-pattern grid (Grating Replica 607, Ted Pella) was used to calibrate TEM imaging between 9.7kx-59kx. Diffraction rings from evaporated gold (Combined Test Specimen 638, Ted Pella) were used to calibrate SAED measurements. STEM/EDS weight percents were calibrated with a microanalysis thin film standard (SRM 2063a, National Institute of Standards and Technology, Gaithersburg, MD), and were found to be accurate to within 0.2, 0.9, and 2.4 weight percent for magnesium, silicon, and iron, respectively. For sample analyses, elemental weight percent ratios to silicon were calculated to minimize the effect of varying background contribution and proximity to copper grid bars.

TEM measurements of fiber morphology and width were used together with SAED and EDS data to classify NOA fibers into five categories: 1) chrysotile asbestos, 2) polygonal serpentine, 3) antigorite blades, 4) lizardite scrolls, 5) lizardite laths. Fiber width measurements for bundles and mats pertained to the average fibril width within the structure.

Morphological classifications of serpentine fibers were defined based on observations from the mineralogy literature. In the preferred orientations that would be observed in a typical

environmental sample analysis, chrysotile fibrils are distinguished by their uniform parallel sides, 5-10 nm central canals, diameters of 20-50 nm, 0.72 nm fringes, and often, uniform end terminations; polygonal serpentine fibers exhibit larger fiber widths of 50-400 nm wide, with irregular, thin canals and often irregular fiber terminations [48] [9] [49]. Published TEM data for antigorite blades in preferred orientation suggest they are massive, with jagged end terminations and non-parallel sides [50] [47]. Fibers with wide, electron-thin interiors and skewed edges are suggestive of fragments of lizardite sheets curled up into loose "scrolls" [51] or "double tubes" [52]; lizardite laths are massive, elongated, blocky fragments.

SAED overlays for Serpentine Minerals

SAED for NOA-related minerals were simulated using a JAVA-based crystallography computer program (JEMS, Version 3.8326, Interdisciplinary Center for Electron Microscopy, École Polytechnique Fédérale de Lausanne). Crystal input files for lizardite, antigorite, talc, muscovite, clinochlore, forsterite, enstatite, tremolite, anthophyllite, and sepiolite were created using literature data from a public database [53].

SAED for serpentine minerals with rotated crystal planes about their fiber axes (chrysotile, polygonal serpentine, and lizardite scrolls) were simulated by combining JEMS-simulated SAED patterns and SAED and XRD data from the literature. Chrysotile SAED patterns were generated for the two most common stacking sequences, clino- and ortho-chrysotile. Quantitative, even-row SAED reflections for clino-chrysotile and ortho-chrysotile were obtained from published XRD data for each polytype [54] [34] [55]. These spot locations were confirmed against published chrysotile SAED patterns [56] [57], and also an approximate JEMS simulation of cylindrical chrysotile created by superimposing reflections from a chrysotile sheet [58] in 001, 010 and 0$\underline{1}$0 zone axis orientations. Odd-row streak positions were obtained from SAED patterns from the literature [56]. Finally, the patterns were confirmed against measured SAED obtained from a chrysotile standard (SRM 1866a, National Institute of Standards and Technology).

Polygonal serpentine SAED were assumed to be similar to chrysotile SAED, but with discrete, odd-row spots and weaker streaks, due to their more ordered rotation [56] [55] [37]. To this end, clino- and ortho-polygonal serpentine overlays were generated by adding even-row reflections from the corresponding chrysotile polytype overlays to the 001 zone axis pattern of lizardite-1T [59]. Polygonal serpentine specimens have been observed to exhibit stacking resembling either polytype [60].

SAED patterns from lizardite scrolls exhibit slightly different even-row reflections and streaking compared to chrysotile, with some inconsistencies (varying spot intensities, split reflections) due to their variable, curled edges [51]. The SAED overlay for lizardite scrolls was created by superimposing 20l and 202-type spots from a 010 lizardite-1T zone axis pattern (orthohexagonal indexing) on the 001 pattern. This overlay is similar to that for polygonal serpentine, except with fewer visible 20l spots.

Graphics software (Photoshop CS5, Adobe, San Francisco, CA) was used to convert these JEMS patterns into simplified overlays (Figure 5), which could be then rotated and superimposed upon measured SAED patterns using the "screen" layer function.
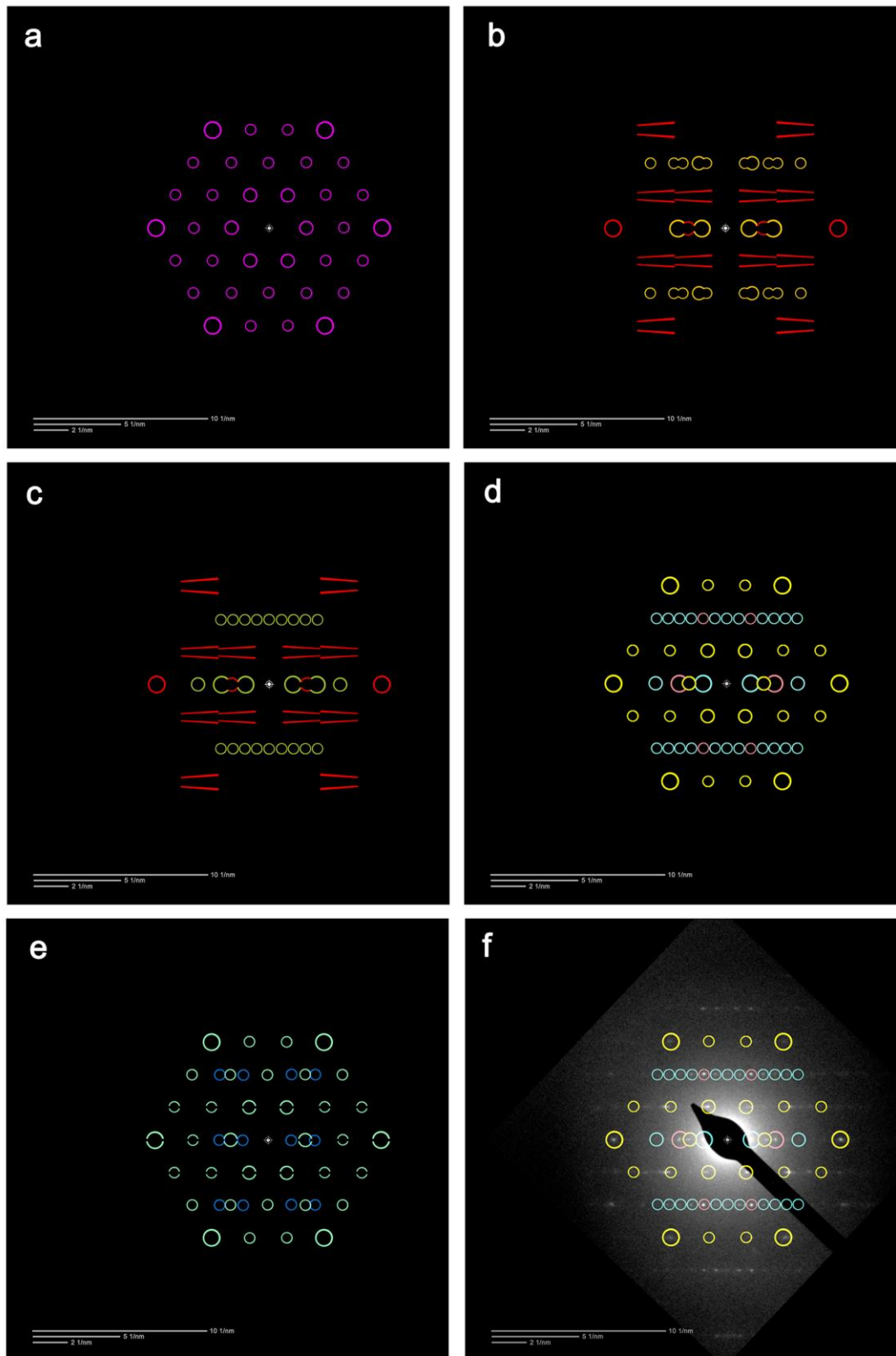
Figure 5. SAED overlays for rapid screening of NOA fibers: a) lizardite, 001 zone axis b) clino-chrysotile c) ortho-chrysotile d) polygonal serpentine (ortho) e) lizardite scrolls f) SAED from NOA fiber (Rock C) with match to polygonal serpentine (ortho).

ESEM/EDS

ESEM/EDS was conducted with an FEI XL30 Environmental SEM (Eindhoven, The Netherlands) with a large-field gaseous secondary electron (GSE) detector, tungsten emission source, and an EDS analyzer with 30 mm^2 silicon drift X-ray detector (Noran System Seven, Thermo Fisher Scientific, Middleton, WI). Samples were analyzed uncoated on standard SEM mounts with double-sided, adhesive carbon tabs at a working distance of 10 mm and an accelerating voltage of 15-20 kV. To improve resolution and minimize charging effects, 0.5-1.0 mbar of water vapor was injected into the SEM chamber with no pressure-limiting aperture. Spatial calibration of the imaging system was calibrated from 50x-80kx with a NIST traceable standard (CDMS-0.1T, Ted Pella, Redding, CA).

RESULTS

Optical Microscopy

Under the stereozoom microscope, many of the cracks and fractures in the analyzed rocks were filled with banded, cross-fiber structures. Probing of cracks in Rocks A and B with tweezers yielded mostly powdery flakes (Figure 2b) and brittle, glassy shards (Figure 3c), as well as a few regions with silky, white tufts (Figure 3b). PLM analyses of subsamples from the latter regions yielded bundles of fibrils with characteristic chrysotile birefringence and asbestiform morphology (Figure 3d-e). In most cases, however, PLM yielded thick, blocky flakes (Figure 2c), or elongated but non-asbestiform structures which were too complex to resolve internal constituents or fibril ends (Figure 3f). Dispersion staining colors obtained from the edges of these structures correspond to slightly higher refractive indices than typical for chrysotile (n_d = 1.56-1.57) (Figures 2d, 3g).

Subsamples from cross-fiber veins in Rock C yielded splintery, white tufts, observed with PLM to be thick, rigid bundles with some fiber colors consistent with chrysotile, n_d = 1.55-1.56 (Figure 4b-d). Others were too thick to yield strong colors in PLM.

For all three rocks, the most prominent NOA particles in the PLM slide preparations were 100-300 um in size, though thinner fiber bundles (10-25 um wide and 20-200 um long) were marginally visible also.

TEM/SAED and STEM/EDS

TEM images and SAED patterns were acquired for 94 NOA fibers from the three rock samples. Measured fibril width, SAED layer line spacing, typical morphology and SAED characteristics, assigned fiber class, and percent clino- and ortho- polytypes are summarized in Table 1. 58 (62%) of the NOA fibers were classified as chrysotile, 32 (34%) were classified as polygonal serpentine, 2 (2%) were classified as lizardite scrolls, and 2 (2%) were classified as lizardite laths. No antigorite fibers were identified; a few fibers resembling antigorite morphology were too thick to yield adequate SAED. STEM/EDS data were collected for 78 of the 94 fibers. Calculated ratios of magnesium, iron, and aluminum to silicon are summarized in Table 1.

The observed morphologies of these NOA fibers generally matched the criteria set in the Methods section, though chrysotile fibril walls were occasionally irregular due to adhered rock matrices. A few, unusually short, low-aspect polygonal serpentine fibers were observed (see image in Table 1) similar in appearance to those reported by Andreani et al. [61].
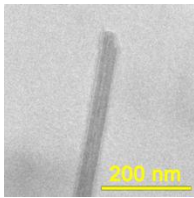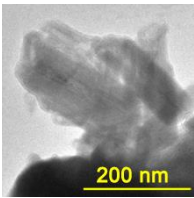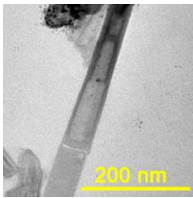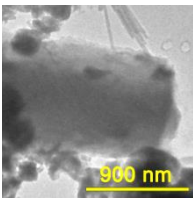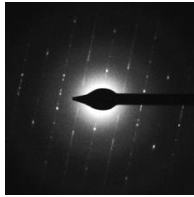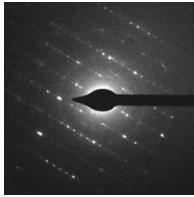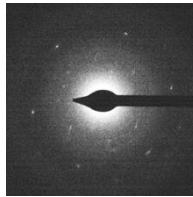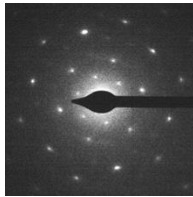
Mean fiber widths for chrysotile and polygonal serpentine were significantly different (42 and 167 nm, respectively; $p \ll 0.05$), though the tails of the measured distributions overlapped at approximately 90 nm (Table 1, Figure 6). Lizardite scroll widths were not significantly different than chrysotile (42 and 37 nm, respectively; $p=0.6$), confirming that confusion between the two polymorphs is possible [51]. Lizardite laths were non-asbestiform, low aspect, and variably but significantly wider than chrysotile (width range = 110-900 nm; $p \ll 0.05$).

SAED overlays provided good matches to experimental SAEDs from the NOA samples (e.g., Figure 5f). In addition to the sharper odd-row reflections expected for polygonal serpentine, it also typically exhibited stronger, sharper even-row reflections than chrysotile as well. Figure 7 shows a cluster of mixed serpentine phases from Rock B containing a single chrysotile fibril, a chrysotile bundle, and a thicker polygonal serpentine fiber with distinct SAED reflections in all rows. Other polygonal serpentine fibers exhibited discontinuous variations in the number of wall layers (Figure 8a), strong ortho-type SAED symmetry (Figure 8b), and isolated walls, possibly crushed during sample preparation, with equidistant center-row SAED reflections and wide spacing consistent with lizardite sheets at an oblique angle to the beam (Figure 8c). Other thick, lizardite laths in preferred orientation exhibited weaker SAED with hexagonal symmetry (see image in Table 1). Thin, lizardite scroll SAEDs exhibited the weakest and most variable spots (Table 1). Non-fibrous species identified by TEM/SAED/EDS included muscovite and talc.

Measured SAED row spacings averaged 1.9 +/- 0.2 nm^{-1} overall, and did not differ significantly between fiber types (all $p>0.05$; lizardite laths differed, but with low statistical power, $n=2$) (Table 1). This average value is in agreement with the theoretical spacing of $1/a$ (=1/0.53 nm) for both lizardite and chrysotile. Even-row reflections indicative of either monoclinic stacking sequences, or less-commonly, orthogonal stacking, were observed in approximately 30% of the SAED patterns (Table 1). The remainder exhibited partially streaked, 2nd-row spots deviating from the pure clino- or ortho-polytype positions, likely due to variable layer stacking geometry [34] or oblique fiber axis angles (see Discussion).

Initial EDS maps revealed that nearly every particle visible on the TEM grids possessed a similar elemental composition. Ratios of magnesium, iron, and aluminum to silicon averaged 0.97, 0.13, and 0.004, respectively. Chrysotile and polygonal serpentine fibers possessed significantly different iron/silicon ratios (0.08 and 0.22, respectively; $p<0.05$) (Table 1). Lizardite laths also exhibited significantly higher aluminum/silicon ratios than chrysotile and polygonal serpentine ($p<0.05$). No other concentration differences were significant between serpentine fiber types. Weight percents on the order of 1% were occasionally recorded for sulfur, chlorine, manganese, or chromium.

Table 1. TEM/SAED/EDS serpentine fiber classifications and average measured parameters.

	Serpentine fiber type	Chrysotile	Polygonal serpentine	Lizardite scroll	Lizardite lath
	n	58	32	2	2
TEM/ morph- ology	typical TEM image				
	fiber width (nm) [a]	42 +/- 16	167 +/- 71	37 +/- 7	505 +/- 559
	central canal	sharp, uniform	thin, irregular	wide, irregular	none
	fiber termination	rounded/ uniform	angular/ irregular	irregular	square
	fiber side edges	parallel	parallel	irregular	irregular
SAED	Typical SAED				
	even-row spots	weak	strong	weak	strong
	odd-row spots	none	weak	weak	strong
	odd-row streaks	strong	weak	weak	none
	row spacing (nm^{-1}) [a]	1.9 +/- 0.2	1.9 +/- 0.2	1.9 +/- 0.1	1.8 +/- 0
	% clino-	16	19	--	--
	% ortho-	10	16	--	--
	% disordered or inclined fiber	74	66	--	--
STEM/EDS	Mg/Si [a]	0.97 +/- 0.26	0.96 +/- 0.21	1.13 +/- 0.15	1.02 +/- 0.03
	Fe/Si [a]	0.08 +/- 0.08	0.22 +/- 0.31	0.15 +/- 0.21	0.18 +/- 0.07
	Al/Si [a]	0.00 +/- 0.01	0.00 +/- 0.01	0 +/- 0	0.04 +/- 0.06

[a] mean +/- std. dev.

TEM grid preparations generally did not exhibit the large particles observed in the PLM subsamples. A few large particles observed in the TEM were 10-20 um wide, but most measured structures were 10-1,000 nm wide, 1-3 orders of magnitude smaller (Figure 6). The few larger particles investigated by TEM were generally too thick for resolving interior morphology or SAED, except for thinner protrusions around their edges.
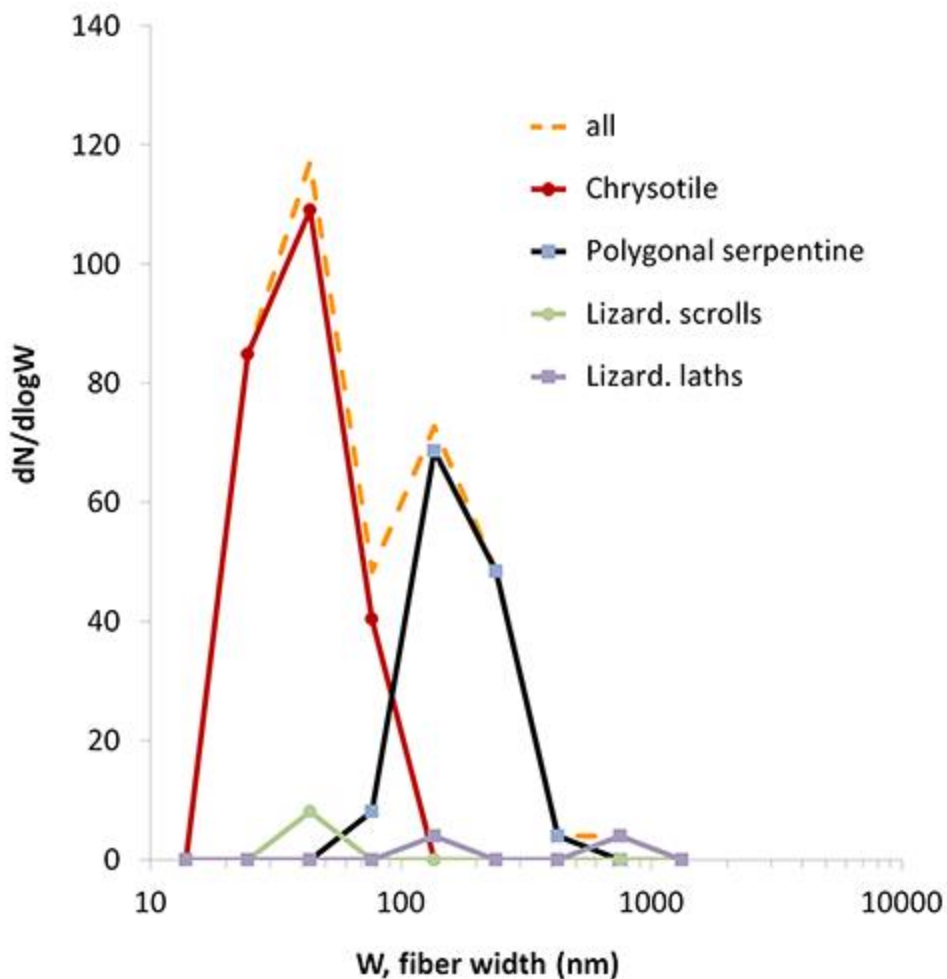
Figure 6. Measured fiber width distribution for all fibers, and for each NOA fiber class as determined by SAED. dN/dlogW is the log-normalized count for each of 9 size bins, with each point plotted at the size bin midpoint.

ESEM/EDS

Figure 9 shows ESEM images of various surface morphologies observed on thick NOA fibers: non-asbestiform sheet structures (Figure 9a), bundles of asbestiform fibrils (Figure 9b), or more complex particles with both non-asbestiform (prismatic, bladed, and amorphous) and asbestiform constituent structures (Figure 9c-f). The complex, elongated particles were typically 10-25 um wide, and similar in gross morphology to fibers which could not be resolved with PLM (Fig. 3 f-g) or TEM. These fibrous intermixtures are consistent with SEM images of serpentine fibers from NOA deposits in El Dorado County, California [30] [62]. The splintery fibers from Rock C (Figure 4) showed a tendency to split into rigid, thinner bundles and curved, asbestiform fibrils at higher SEM magnifications (Figure 9f).

The largest particles visible in the SEM preparations were similar to those in the PLM preparations, approximately 200 um. The smallest fiber structures observed in the SEM were on
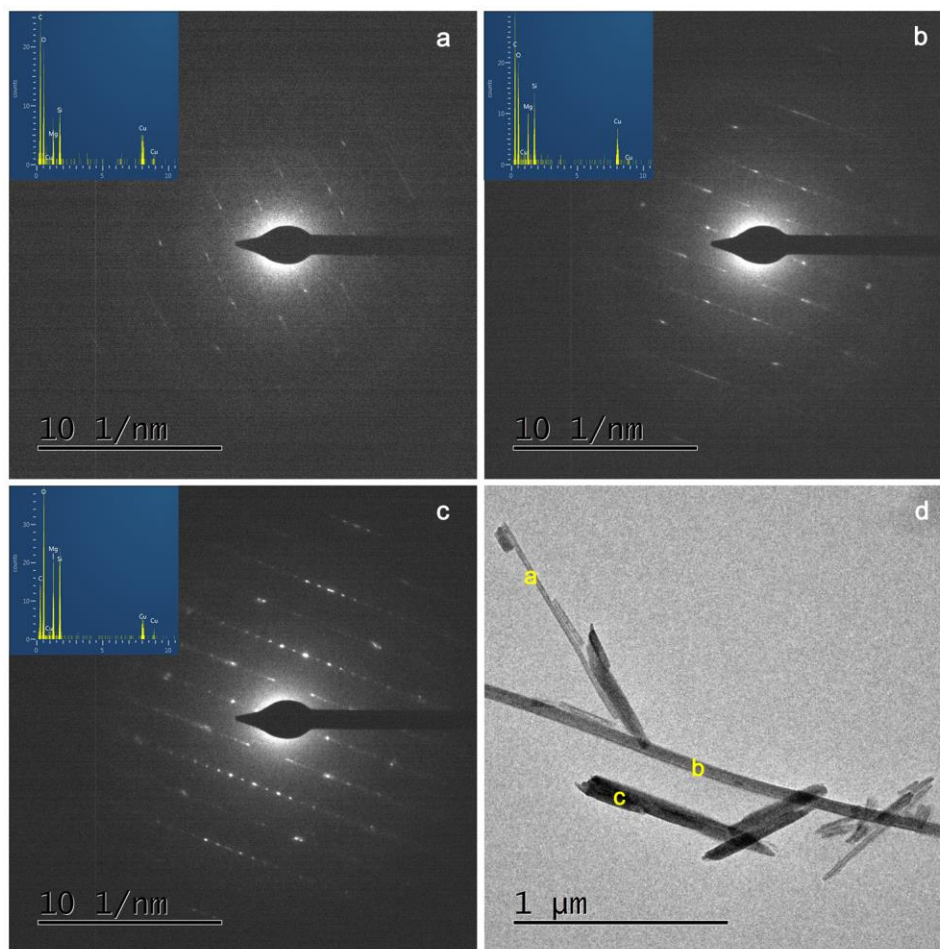
Figure 7. TEM/SAED and STEM/EDS of cluster of mixed serpentine phases from Rock B: a) single chrysotile fibril, b) chrysotile bundle, c) polygonal serpentine fiber, d) 26.5 kx image showing acquisition locations (a)-(c).

the order of 0.1 um, which overlaps most of the 0.01 – 10 um size range analyzed by TEM.

Nearly every analyzed fiber and amorphous region in these rock subsamples exhibited strong magnesium and silicon EDS peaks, with minor iron, and occasionally minor aluminum (Figure 9). These results are consistent with those obtained with TEM/EDS. Although phase identification with SEM/EDS was not possible, these elements are consistent with the serpentine minerals, enstatite, and talc.

DISCUSSION

SAED overlays enabled rapid discrimination between superficially similar chrysotile, polygonal serpentine, and lizardite scroll SAEDs. In addition, Figure 6 suggests that serpentine fibrils >100 um wide could be flagged in TEM screening analyses as being potentially non-chrysotile, although fiber width distributions from chrysotile and polygonal serpentine overlapped slightly.
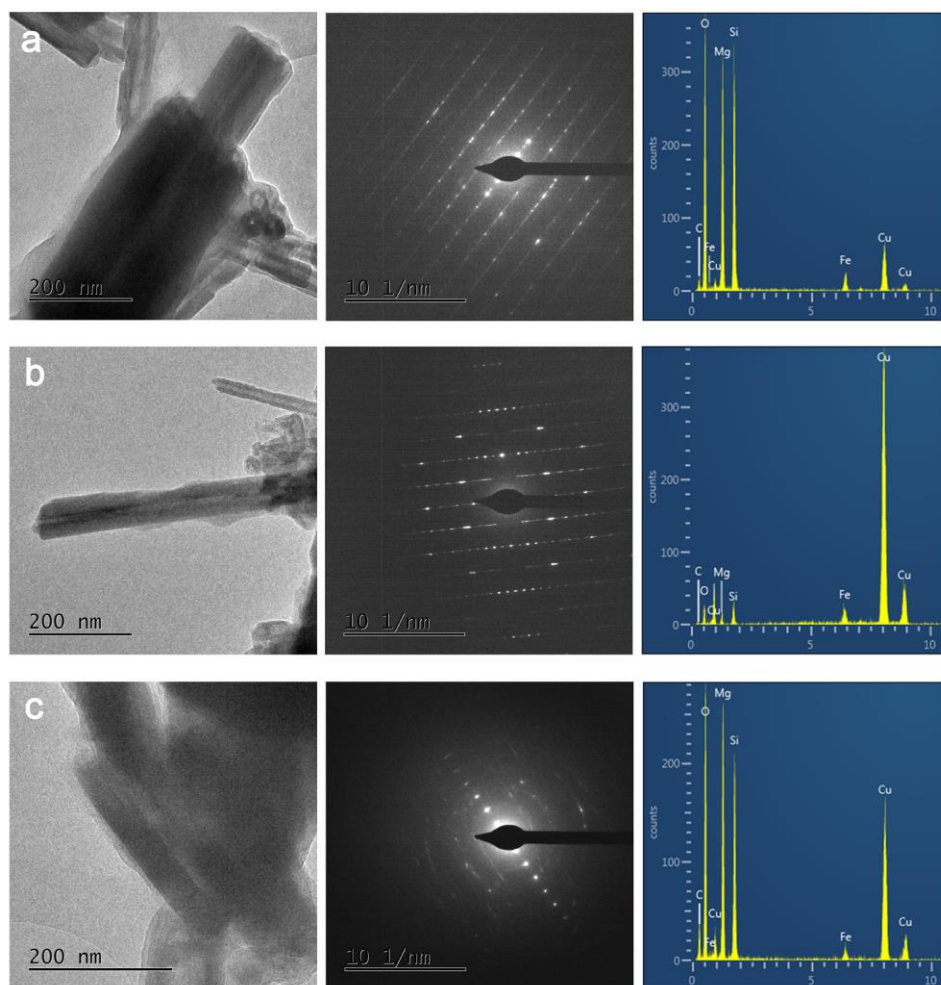
Figure 8. TEM/SAED and STEM/EDS of polygonal serpentine fibers from Rock A with a) discontinuously varying wall thicknes (97 kx), b) strong orthogonal symmetry in SAED (image = 97 kx), c) very wide row spacing in SAED, consistent with crushed lizardite sheet walls at oblique angle to beam (image = 135 kx).

Average EDS differences between serpentine phases were confirmed to be generally insignificant [28] compared to natural variability within individual serpentine phases [38]. The lower iron and aluminum concentrations measured in chrysotile may have been due to lower x-ray counts for the thinner chrysotile fibrils, which likely contributed to non-detects and lower averages for these minor elements.

Approximately a third of the fibers in this study were classified as polygonal serpentine. Although the actual prevalence is uncertain due to non-representative sampling, many of the veins in these rocks broke into shards when probed, consistent with polygonal serpentine's splintery texture [56] [37] and pseudo-fibrous habit [8]. Polygonal serpentine intermixed with chrysotile has been observed in serpentinite veins within Franciscan Complex regions [9] and in the Italian Alps [63].

The measurement of SAED row spacing advocated by standard asbestos methods [23] can be
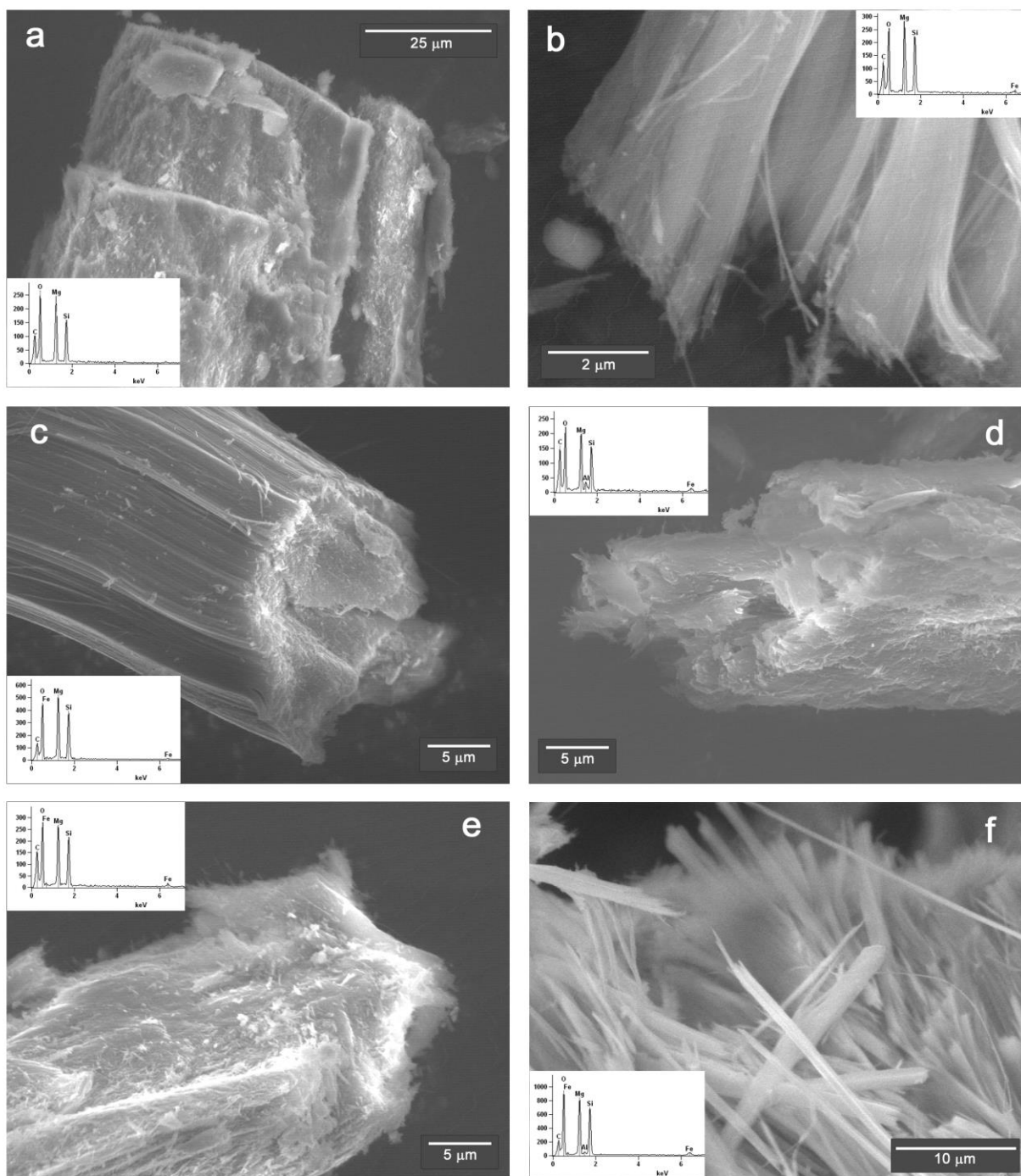
Figure 9. EDS data and ESEM/GSE images showing different surface morphologies of thick NOA fibers. a) layered sheets (Rock A, 2.5kx); b) asbestiform bundles (Rock B, 24kx); c) intergrown blades and asbestiform fibers around an cylindrical, amorphous core (Rock B, 6kx); d) intergrown blades and asbestiform fibers in large fiber with parallel sides (Rock B, 6kx); e) intergrown blades and asbestiform fibers in irregular but elongated particle (Rock B, 6kx); f) rigid, thin bundles and curved, asbestiform fibrils at end of large, splintery fiber (Rock C, 6kx).

compromised if the angle between beam and fiber axis is not 90 degrees. In this study, deviations of up to +40% were observed from the 1.9 nm^{-1} layer line spacing expected for chrysotile and lizardite. Subsequent investigation revealed that row spacing decreased to the expected value after adjusting the stage tilt. Non-orthogonal fiber angles likely resulted from stage tilts implemented for optimal EDS, warped carbon films, and/or fibers emerging at oblique angles from serpentine rock matrix particles. Oblique tilting of cylindrical or helical structures can also cause asymmetry in SAED quadrants, streaked and arc-shaped odd-row spots, and shifted even-row reflections [64] [65]. Thus, although the SAED symmetry of chrysotile fibers is relatively invariant with tilt, tilting to a minimum SAED row spacing is prudent before using row spacing as a diagnostic.

Because of different particle sizes observed due to differing preparations and microscope resolutions, PLM analyses essentially investigated a different population of particles than did TEM analyses. Possibly, larger NOA particles were too heavy for the TEM grid support films, as evidenced by the many observed broken grid squares. Other particles may have been too large to adhere to the TEM grids at all. The low prevalence of large particles in the TEM may have contributed to the observed scarcity of more typically massive serpentine minerals such as lizardite and antigorite. Such an under-representation of non-asbestiform, larger particles could lead to overestimates of asbestos mass percentages in aggregate analyses by TEM. Different mechanical pulverization procedures likely could break down large particles more efficiently than the manual grinding conducted in this study, which would result in a greater proportion of aggregate being retained by TEM grids. However, such fine pulverization is not recommended by recently proposed NOA grinding methods, which specify a majority of particles sized 75-250 um [11]. Missing large particles would be most problematic for assessments of asbestos mass concentration for toxic materials transport, or for sites where high-energy fiber liberation from larger particles is a concern. In such cases, supplemental ESEM/EDS analyses could reveal whether asbestos is prevalent in the larger, more complex NOA particles. On the other hand, for investigations of respirable fiber number concentrations released by low-energy site activities, the finer fraction of NOA particles in the TEM may be desirable.

The broken TEM grid squares observed in these NOA filtrations were somewhat sample dependent. Specifically, the filtered sub-samples from Location 1(Rocks A and B) appeared to receive a lighter, weaker carbon film coating than Rock C from Location 2, even though they were coated simultaneously. Possibly, the Location 1 rocks contained an organic substance which was distributed across the filter during filtration and prevented adsorption of the vaporized carbon. If so, heating of the NOA samples to a moderate temperature in a muffle furnace prior to carbon coating could be used to remove the organic matter. This hypothesis is consistent with the beam-sensitive globules that were associated with many of the particles in the microdrop preparations from Location 1. In general, the filtration preparations exhibited superior particle deposition uniformity compared to the microdrop preparations.

ESEM/EDS of large (20-200 um long, 10-25 um wide), complex NOA particles enabled resolution of intermixed asbestiform and non-asbestiform fiber structures on their surfaces that were not resolvable with PLM or TEM. The constituent asbestiform fibers within these structures could be important if liberation by a high-energy activity (e.g. demolition) is a concern. If so, both PLM and TEM methods may yield false negatives. The particles themselves were often elongated but non-asbestiform (Figures 3f, 9c), and thus ambiguous with regards to asbestos

classification. Some PLM and TEM asbestos identification methods specify only 3:1 or 5:1 aspect ratio and typical morphology [20] [23] [22], while others specify asbestiform morphology [18]. Particles 10-25 um wide are likely to exist in NOA aggregate samples prepared by standard mechanical grinding methods [20] [18], but are probably too large to be aerosolized by "releasable" NOA preparation methods [66] [67].

CONCLUSIONS

Although superficially similar, non- asbestos serpentine fibers (polygonal serpentine, lizardite laths and scrolls) can be differentiated quickly from chrysotile using TEM morphology, fiber widths, and reference SAED overlays. Tilting serpentine fibers to a minimum SAED row spacing improved row spacing diagnostic measurements.

Due to differing preparation methods and microscope resolutions, TEM subsamples represented a distinct, smaller population of NOA particles (0.01-10 um) compared to PLM subsamples (10-300 um). A higher asbestos percentage in the fine fraction could bias TEM bulk percent asbestos determinations.

Qualitative ESEM/EDS imaging at intermediate magnifications revealed large, elongated, non-asbestiform particles with asbestiform fibers on their surfaces. These surfaces were not resolvable with transmitted techniques (PLM and TEM). The relevance of these complex particles depends upon the asbestos definition and size fraction specified by a given NOA investigation. In cases where asbestos concentrations of larger particles are required, these fibers could potentially be more finely pulverized for TEM.

Future work will apply these analytical approaches to natural occurrences of other fibrous minerals which exhibit asbestiform- and non-asbestiform habits, different rotational symmetry, twinning, or non-uniform orientations within bundles, including amphiboles (e.g. tremolite) and 2:1 clays (e.g. palygorskite) [39] [68]. In addition, the practicality of electron back-scatter diffraction (EBSD) techniques will be explored for NOA samples. If suitable sample preparation methods could be developed, EBSD of NOA would combine the beneficial surface analysis capabilities of SEM/EDS with crystallographic phase identification.

REFERENCES

[1]   A. F. Cook and H. Hoas, "The landscape of asbestos: Libby and beyond," *Journal of Risk Research,* vol. 12, p. 105–113, 2009.

[2]   K. Ladd, "El Dorado Hills Naturally Occurring Asbestos Multimedia Exposure Assessment El Dorado Hills, California: Preliminary Assessment and Site Inspection Report, Interim Final," Ecology and Environment, Inc. Job #001275.0440.01CP, prepared for US EPA R9, 2005.

[3]   U.S. Environmental Protection Agency, "Soil, Sediment and Surface Water Sampling, Sumas Mountain Naturally-Occurring Asbestos Site, Whatcom County, Washington," Region 10, Office of Environmental Assessment, Seattle, WA, 2009.

[4]   B. J. Buck, D. Goossens, R. V. Metcalf, B. McLaurin, M. Ren and F. Freudenberger, "Naturally Occurring Asbestos: Potential for Human Exposure, Southern Nevada, USA," *Soil Sci. Soc. Am. J.,* vol. 77, p. 2192–2204, 2013.

[5]   B. S. Van Gosen and J. P. Clinkenbeard, "Reported Historic Asbestos Mines, Historic Asbestos Prospects, and Other Natural Occurrences of Asbestos in California," U.S. Geological Survey, Reston, Virginia, 2011.

[6]   M. Bailey, "Regulated And Unregulated Fibrous Amphiboles Of The Franciscan Formation Found In The Greater San Francisco Bay Area," in *Assessment, Monitoring and Mitigation of Naturally Occurring Asbestos (NOA) Hazards in the Western U.S., Association of Environmental & Engineering Geologists Symposium*, Oakland, CA, 2012.

[7]   M. Ross, "Geology, Asbestos, and Health," *Environmental Health Perspectives,* vol. 9, pp. 123-124, 1974.

[8]   California Department Of Conservation, "Guidelines For Geologic Investigations Of Naturally Occurring Asbestos in California," Special Publication 124, 2002.

[9]   M. Andreani, A. Baronnet, A.-M. Boullier and J.-P. Gratier, "A microstructural study of a "crack-seal" type serpentine vein using SEM and TEM techniques," *Eur. J. Mineral.,* vol. 16, p. 585–595, 2004.

[10] J. Wagner and G. Casuccio, "Spectral Imaging and Passive Sampling to Investigate Particle Sources in Urban Desert Regions," *Environ. Sci.: Processes Impacts,* vol. 16, pp. 1745-53, 2014.

[11] California Air Resources Board, "Good Field Sampling and Laboratory Practices - Test Method 435: Determination of Asbestos Content of Serpentine Aggregate," in *Assessment, Monitoring and Mitigation of Naturally Occurring Asbestos (NOA) Hazards in the Western U.S., Association of Environmental & Engineering Geologists Symposium*, Oakland, 2014.

[12] J. De Vita, S. Wall, J. Wagner, Z.-M. Wang and L. E. Rao, "Determining the Frequency of Asbestos Use in Automotive Brakes from a Fleet of On-Road California Vehicles," *Environ. Sci. Technol.,* vol. 46, p. 1344–1351, 2012.

[13] M. Harper, "10th Anniversary critical review: Naturally occurring asbestos.," *J. Environ. Monit.,* vol. 10, p. 1394–1408, 2008.

[14] G. Meeker, A. Bern, I. Brownfield, H. Lower, S. Sutley, T. Hoefen and J. Vance, "The Composition and Morphology of Amphiboles from the Rainy Creek Complex, Near Libby, Montana," *American Mineralogist,* vol. 88, pp. 1955-1969, 2003.

[15] R. Lee, B. Strohmeier, K. Bunker and D. Van Orden, "Naturally occurring asbestos - A recurring public policy challenge," *J. Haz. Mat.,* vol. 153, p. 1–21, 2008.

[16] M. Gunter, "Defining asbestos: Differences between the built and natural environments," *Chimia ,* vol. 64, p. 747–752, 2010.

[17] D. Van Orden, K. Allison and R. Lee, "Differentiating amphibole asbestos from non-asbestos in a complex mineral environment," *Indoor Built Environ.,* vol. 17, p. 58–68, 2008.

[18] U.S. Environmental Protection Agency, "Method for the Determination of Asbestos in Bulk Building Materials," U.S. Environmental Protection Agency Method 600/R-93/116, Washington DC, 1993.

[19] A. Wylie, R. Virta and E. Russel, "Characterizing and discriminating airborne amphibole cleavage fragments and amosite fibres: implications for NIOSH method," *Am. Ind. Hyg. Assoc. J.,* vol. 46, p. 197–201, 1985.

[20] California Air Resources Board, "Determination of Asbestos Content of Serpentine Aggregate," CARB Method 435, 1991.

[21] ASTM International, "ASTM D7521-13, Standard Test Method for Determination of Asbestos in Soil," West Conshohocken, PA, 2013.

[22] US Environmental Protection Agency, ""Asbestos-Containing Materials in Schools; Final Rule and Notice"," Federal Register, 40 Code of Federal Regulations Part 763, Subpart E, Appendix E, October 30, 1987.

[23] International Organization for Standardization, "ISO 10312. Ambient Air Determination of Asbestos Fibres—Direct Transfer Transmission Electron Microscopy Method," Geneva, Switzerland, 1995.

[24] Department of Toxic Substance Control, "Interim Guidance: Naturally Occurring Asbestos (NOA) at School Sites," Glendale, CA, 2004.

[25] M. Bailey, "Considerations When Submitting Rock/Soil Samples for NOA Laboratory Analysis," in *Assessment, Monitoring and Mitigation of Naturally Occurring Asbestos (NOA) Hazards in the Western U.S., Association of Environmental & Engineering Geologists Symposium*, Oakland, 2014.

[26] A. Cattaneo, A. Somigliana, M. Gemmi, F. Bernabeo, D. Savoca, D. Cavallo and P. Bertazzi, "Airborne Concentrations of Chrysotile Asbestos in Serpentine Quarries and Stone Processing Facilities in Valmalenco, Italy," *Ann. Occup. Hyg.,* vol. 56/6, p. 671 – 683, 2012.

[27] A. Gualtieri, S. Pollastri, N. Bursi Gandolfi, F. Ronchetti, C. Albonico, A. Cavallo, G. Zanetti, P. Marini and O. Sala, "Determination of the concentration of asbestos minerals in highly contaminated mine tailings: An example from abandoned mine waste of Crètaz and Èmarese (Valle d'Aosta, Italy).," *Am. Mineral.,* vol. 99, pp. 1233 - 1247, 2014.

[28] A. Cavallo and B. Rimoldi, "Chrysotile asbestos in serpentinite quarries: a case study in Valmalenco, Central Alps, Northern Italy.," *Environ. Sci. Processes Impacts,* vol. 15, p. 1341 – 1350, 2013.

[29] RJ LeeGroup, "Evaluation of EPA's Analytical Data from the El Dorado Hills Asbestos Evaluation Project," RJ LeeGroup, Inc, Monroeville, PA, 2005.

[30] G. Meeker, H. Lowers, G. Swayze, B. V. Gosen, S. Sutley and I. Brownfield, "Mineralogy and Morphology of Amphiboles Observed in Soils and Rocks in El Dorado Hills, California," U.S. Geological Survey Open-File Report 2006–1362, 2006.

[31] B. R. Strohmeier, K. L. Bunker, K. E. Harris, R. Hoch and R. J. Lee, "Complementary TEM and FESEM Characterization of Amphibole Particles in Mixed Mineral Dust from Libby, Montana, U.S.A.," *MICROSCOPE,* vol. 55, pp. 173-188, 2007.

[32] J. Harris, "Observations From TEM Analysis of Swift Creek Samples," in *Assessment, Monitoring and Mitigation of Naturally Occurring Asbestos (NOA) Hazards in the Western U.S., Association of Environmental & Engineering Geologists Symposium*, Oakland, CA, 2012.

[33] G. Cressey, J. Spratt and B. Cressey, "Electron and X-Ray Petrography Of an Unusual Serpentine From the Tilly Foster Mine, Brewster, New York," *Canadian Mineralogist,* vol. 31, pp. 447 -458, 1993.

[34] E. J. W. Whittaker and J. Zussman, "The Characterization of Serpentine Minerals by X-ray Diffraction," *Mineralogical Magazine,* vol. 31, pp. 107-126, 1956.

[35] D. R. Veblen and P. R. Buseck, "Serpentine Minerals: Intergrowths and New Combination Structures," *Science,* vol. 206, pp. 1398-1400, 1979.

[36] K. Yada, "Study of Microstructure of Chrysotile Asbestos by High Resolution Electron Microscopy,"

Acta Cryst., vol. A27, pp. 659-664, 1971.

[37] B. A. Cressey and J. Zussman, "Electron Microscopic Studies Of Serpentinites," *Canadian Mineralogist,* vol. 14, pp. 307-313, 1976.

[38] H. Schreier, Asbestos in the Natural Environment, New York: Elsevier Science Publishers, 1989.

[39] P. E. Champness, G. Cliff and G. W. Lorimer, "The identification of asbestos," *Journal of Microscopy,* vol. 108, p. 231–249, 1976.

[40] M. J. Blake, R. Graymer and D. Jones, "Geologic map and map database of parts of Marin, San Francisco, Alameda, Contra Costa, and Sonoma Counties, California: Pamphlet to Accompany Miscellaneous Field Studies MF-2337, Version 1.0," U.S. Geological Survey, 2000.

[41] J. Schlocker, "Geology of the San Francisco North quadrangle, California," U.S. Geological Survey Professional Paper 782, 1958.

[42] S. Ludington, B. C. Moring, R. J. Miller, K. S. Flynn, P. A. Stone and D. R. Bedford, "Preliminary integrated databases for the United States - Western States: California, Nevada, Arizona, and Washington," U.S. Geological Survey Open-File Report OFR 2005-1305, Reston, Virginia, 2005.

[43] California Geological Survey, "GIS Data for the Geologic Map of California," CD-ROM 2000-007, 2000.

[44] B. S. Van Gosen, "Asbestos mines, prospects, and occurrences in the US," U.S. Geological Survey Online, http://tin.er.usgs.gov/asbestos, Reston, Virginia, 2011.

[45] G. Swayze, R. Kokaly, C. Higgins, J. Clinkenbeard, R. Clark, H. Lowers and S. Sutley, "Mapping potentially asbestos-bearing rocks using imaging spectroscopy," *Geology,* vol. 37, pp. 763-766, 2009.

[46] US Geological Survey , "National Gap Analysis Program Land Cover Data- Version 2," http://gapanalysis.usgs.gov/gaplandcover/, 2011.

[47] W. C. McCrone, Asbestos Identification, Chicago: McCrone Research Institute, 1987.

[48] B. Devouard, A. Baronnet, G. Van Tendeloo and A. S, "First Evidence of Synthetic Polygonal Serpentines," *Eur. J. Mineral. ,* vol. 9, pp. 539-546, 1997.

[49] A. Baronnet and E. Belluso, "Microstructures of the silicates: key information about mineral reactions and a link with the Earth and materials sciences," *Mineralogical Magazine,* vol. 66, p. 709–732, 2002.

[50] I. Ribeiro Da Costa, F. J. Barriga, C. Viti, M. Mellini and F. J. Wicks, "Antigorite in deformed serpentinites from the Mid-Atlantic Ridge," *Eur. J. Mineral.,* vol. 20, pp. 563-572, 2008.

[51] F. J. Wicks and E. J. Chatfield, "Scrolling of Thin Crystals of Lizardite: an Expression of Internal Stress," *The Canadian Mineralogist,* vol. 43, pp. 1993-2004, 2005.

[52] G. L. Kalousek and L. E. Muttart, "Studies on the Chrysotile and Antigorite Components of Serpentine," *American Minerologist,* vol. 42, 1957.

[53] R. Downs and M. Hall-Wallace, "The American Mineralogist Crystal Structure Database," *American Mineralogist,* vol. 88, pp. 247-250, 2003.

[54] F. J. Wicks, "Status of the reference X-ray powder-diffraction patterns for the serpentine minerals in the PDF database—1997," *Powder Diffraction,* vol. 15, pp. 42-50, 2000.

[55] F. Wicks and D. O'Hanley, "Serpentine minerals: Structuresand petrology, in Hydrous Phyllosilicates (Exclusive of Micas)," *Reviews in Mineralogy,* vol. 19 , pp. 91-167, 1988.

[56] J. Zussman, G. Brindley and J. Comer, "Electron Diffraction Studies of Serpentine Minerals," *American Minerologist,* vol. 42, pp. 133-153, 1957.

[57] J. Gard, Ed., The Electron Optical Investigation of Clays, London: The Mineralogical Society, 1971.

[58] G. Falini, E. Foresti, M. Gazzano, A. F.Gualtieri, M. Leon, I. G.Lesci and N. Roveri, "Tubular-Shaped Stoichiometric Chrysotile Nanocrystals," *Chem. Eur. J.,* vol. 10, p. 3043 ± 3049, 2004.

[59] S. Guggenheim and W. Zhan, "The effect of temperature on the structures of lizardite-1T and lizardite-2H1," *The Canadian Mineralogist,* vol. 36, pp. 1587-1594, 1998.

[60] A. Middleton and E. Whittaker, "The Structure of Povlen Type Chrysotile," *Canadian Mineralogist,* vol. 14, pp. 301-306, 1976.

[61] M. Andreani, O. Grauby, A. Baronnet and M. Muñoz, "Occurrence, composition and growth of polyhedral serpentine," *Eur. J. Mineral.,* vol. 20, p. 159–171, 2008.

[62] G. A. Swayze, C. T. Higgins, J. P. Clinkenbeard, R. F. Kokaly, R. N. Clark, G. P. Meeker and S. J. Sutley, "Preliminary Report on Using Imaging Spectroscopy to Map Ultramafic Rocks, Serpentinites, and Tremolite-Actinolite-Bearing Rocks in California," California Geological Survey Geologic Hazards Investigation 2004-01 and U.S. Geological Survey Open-File Report 2004-1304, 2004.

[63] M. Mellini, "Chrysotile and polygonal serpentine from the Balangero serpentinite," *Mineralogical Magazine,* vol. 50, pp. 301-5, 1986.

[64] N. Stribeck, "On the determination of fiber tilt angles in fiber diffraction," *Foundations of Crystallography,* vol. A65, pp. 46-47, 2008.

[65] K. Yada, "Microstructures of Chrysotile and Antigorite by High Resolution Electron Microscopy," *Canadidn Mineralogist,* vol. 17, pp. 679-691, 1979.

[66] D. Berman and A. Kolk, "Interim Superfund Method for theDetermination of Releasable Asbestos in Soils and Bulk Materials.," US Environmental Protection Agency Method 540-R-97-028, 1997.

[67] J. R. Kominsky, J. W. Thornburg, G. M. Shaul, W. M. Barrett, F. D. Hall and J. J. Konz, "Development of the Releasable Asbestos Field Sampler," *Journal of the Air & Waste Management Association,* vol. 60, pp. 294-301, 2010.

[68] E. García-Romero and M. Suárez, "Sepiolite-palygorskite polysomatic series: Oriented aggregation as a crystal growth mechanism in natural environments," *American Mineralogist,* vol. 99, p. 1653–1661, 2014 .